Journal of the Mechanics and Physics of Solids 59 (2011) 178–193

Contents lists available at ScienceDirect

Journal of the Mechanics and Physics of Solids

journal homepage: www.elsevier.com/locate/jmps

A theoretical analysis of the breakdown of electrostrictive oxide film on metal

Yuye Tang *, Roberto Ballarini

Department of Civil Engineering, University of Minnesota, Minneapolis, MN 55455, United States

ARTICLE INFO

Article history:
Received 2 September 2010
Received in revised form
19 October 2010
Accepted 8 November 2010
Available online 18 November 2010

Keywords:
Passive/anodic oxide films
Breakdown mechanisms
Thermodynamics
Electromechanical effects
Critical electric field strength

ABSTRACT

Oxide films that form to protect (passivate) metal substrates from corrosive environments can be severely damaged when they are subjected to sufficient levels of electric potential. A continuum mechanics model is presented that captures the intimate electromechanical coupling of the environment and the film responsible for either growth or dissolution of the oxide. Analytical solutions, obtained for a finite-thick film experiencing a uniform electric field, illustrate the existence of a critical combination of electric field strength, initial film thickness and shape, beyond which the passivating oxide can become thin enough to undergo dielectric breakdown, or the substrate can become exposed to the corrosive environment. An experimental procedure is proposed to measure combinations of material properties required by the theoretical model to predict the lifetime of the oxide or to avoid the critical state. Illustrative numerical examples are provided to describe the morphological evolution of oxide films with a periodically wavy surface.

1. Introduction

Passive and/or anodic oxide films that protect a metal substrate from the attack of a corrosive environment may experience and respond to a considerable electric field. For example, improved corrosion and wear resistance of Aluminum can be achieved by thickening the natural oxide through the electric field involved in the anodizing process (Wernick et al., 1987); however, galvanic couples formed in the presence of electrolytes lead to electric potential differences that can consume the oxide layers and lead to corrosion (McCafferty, 2010). Studies (Kaesche, 1960; Leckie and Uhlig, 1966; Martin et al., 2007, 2009) showing that the corrosion protection is destroyed at a critical electric potential have provided key insights for clarifying the breakdown mechanism of oxide films in practical applications. Corresponding physical and computational models that can characterize and predict the breakdown phenomena, however, are lagging. Using a thermodynamic framework, Sato (1971) suggested that mechanical failure of the film can result from brittle cracking or plastic deformation driven by the high levels of electromechanical stress that can be generated by the electric field. Sato's model is limited by the assumption of a homogeneous isotropic film pressure, characteristic of a fluid medium and not a solid, and it does not predict the morphological evolution of the film and the associated stress field. Furthermore, it failed to consider the primary electromechanical coupling involved, electrostriction in the passive oxide films (Heuer et al., Private Communication). The degradation of an oxide film produced by the change of its surface shape when subjected to thermal mismatch-induced residual stress was investigated (Srolovitz, 1989; Yu and Suo, 2000; Liang and Suo, 2001; Yang, 2006). These models, however,

* Corresponding author. Tel.: +1 646 709 1858.
E-mail address: Yuye.Tang@gmail.com (Y. Tang).

0022-5096/$ - see front matter © 2010 Elsevier Ltd. All rights reserved.
doi:10.1016/j.jmps.2010.11.002

do not include electromechanical effects. Du and Srolovitz (2004) and Song and Yang (2006) did consider how an imposed electric field could compromise the morphological stability of an oxide film, but they also did not include the effects of electrostriction. This paper investigates and demonstrates the possibility that the intimate coupling between the environment, the electric field and elasticity, changes the morphology of the oxide film in ways that can lead to dielectric breakdown of the oxide film or exposure of the substrate to the corrosive environment.

The problem under investigation, shown in Fig. 1a, involves an electrostrictive oxide thin film formed on a metal surface and in contact with an aggressive liquid or vapor environment. The film and the environment are considered as a composite system with prescribed mechanical and electric boundary conditions. The chemical reaction is assumed to proceed slowly enough that each phase of the composite remains in a quasi-static equilibrium. Nonequilibrium prevails at the interface between the two phases, where the exchange of atoms can cause the film to either grow or dissolve. We suggest that the functionality of the protective coating can be compromised as a result of its thickness being reduced to a critical level, or by its surface shape changing to a wave of critical amplitude. Be it by depletion of the film, dielectric breakdown or by cracking as a result of ever increasing stress concentration, the metal substrate will eventually be exposed to the corrosive environment. These two scenarios would be consistent with the failures observed in experiments (Martin et al., 2007, 2009).

The evolution of the film's morphology and the stresses that develop within it can be derived using nonequilibrium thermodynamics (NET), a theoretical framework capable of characterizing transport phenomena in systems that are not in global equilibrium such as the propagation of a sharp shock front within a domain. The solution procedure is summarized in a step by step manner in Section 2. The electromechanical governing equations for small deformations, from which one derives the instantaneous electric and stress fields in the composite system, are presented first. Next, the thermodynamic driving force (TDF) at the film–environment interface that drives the variation of the film's instantaneous profile is introduced with associated electric and stress field input variables. Since none of the TDFs developed for the moving shock problem (Abeyaratne and Knowles, 1990; Jiang, 1994; James, 2002) can be applied to the problem studied here, the TDF acting at a moving discontinuous surface in quasi-electrostatic thermoelastic continua (Fig. 2), together with the corresponding equilibrium equations and boundary conditions, are derived in Appendix A. The derivation of the large deformation case relies on a series of global balance and energy laws. The TDF acting along the film–environment interface is obtained for small deformations in Section 2 by generalizing the TDF in Appendix A to include changes in the chemical and surface energies within the closed system. Finally, the film's morphology is updated by applying the kinetic relation between the speed of the moving film–environment interface and the TDF that is imported from the point of view of material science (Yu and Suo, 2000; Liang and Suo, 2001; Prevost et al., 2001). Note that the NET framework described in Section 2 represents a more general approach for studying the breakdown of oxide films than those currently available. Finite element formulations could be established for the equations that comprise the model listed here that also consider the effects of flexoelectric stresses (due to field gradients, strain gradients, or gradients in dielectric properties through the film) as well as the initiation and growth of cracks or plastic deformation.

In order to clarify the breakdown mechanism and sort out the essential factors determining the corrosion resistance, the analytical solution for the evolution of the thickness and shape of a film under the assumption of a uniform and constant electric field is presented in Section 3. The implications of the analytical results, together with illustrative numerical examples, are explored in Section 4. In particular, the existence is proved of a critical combination of electric field strength,

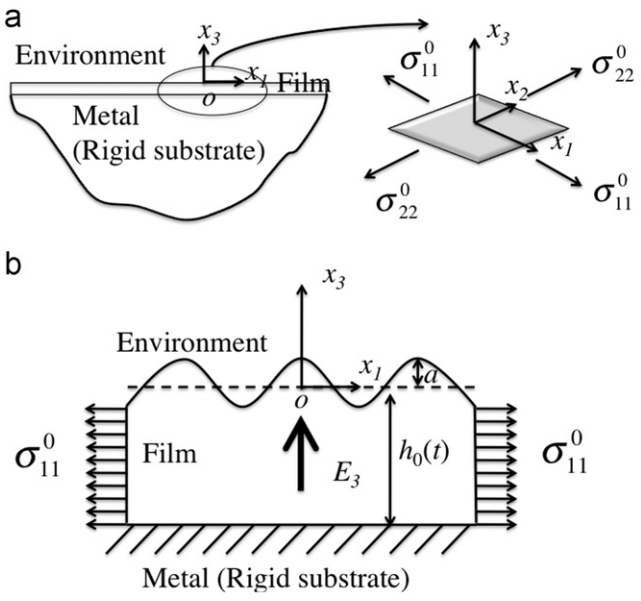

Fig. 1. An oxide film on a metal substrate in contact with a corrosive environment: (a) schematic view of the entire system, and the in-plane stress states in the flat film; (b) close-up view of the film with wavy surface.

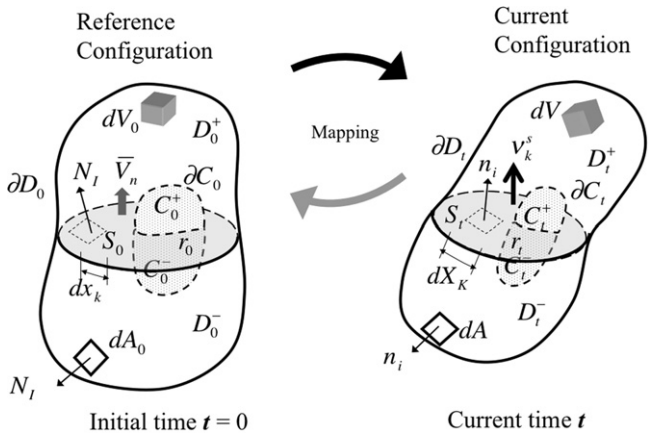

Fig. 2. Thermoelectroelastic continua with a singular moving surface. The direction of the surface normal N_I and n_i on the moving surface is from $-$ to $+$.

initial film thickness and density of surface roughness that could result in breakdown of the oxide film. An experimental procedure is proposed to measure certain combinations of material properties associated with the critical conditions. The results of this study could guide the design of protective coatings.

2. Problem formulation and solution procedure

The film and the environment are considered as two thermoelectroelastic materials separated by a moving interface (Fig. 1). The chemical reaction at the interface proceeds slowly, so that the composite system is under isothermal and quasi-static conditions. This enables the derivation of the electric and stress fields in each phase by application of equilibrium conditions. The resulting simplified nonequilibrium TDF at the interface is affected by current electric and stress field inputs and drives surface motions of the film through a kinematic relation. The instantaneous profile and internal stresses of the film can be resolved by repeating the detailed three-step procedure listed below.

Step 1. *Solution for the field variables*: The field variables in the film and in the environment can be obtained by solving a boundary value problem, which consists of a set of local equations, jump and boundary conditions (for finite deformation, Eq. (59a), (59b), (59d), (60a), (60b), (60d), (53) in Appendix A), and a free energy function.

The problem considered here involves small deformation, for which the governing equations are significantly simplified (Kuang, 2009; Jiang and Cao, 2010). Note that certain variables used subsequently are labeled differently than their large deformation counterparts in Appendix A: $\phi, D_i, E_i, q_e, w_e, w_e^{int}$ represent the electric potential, the electric displacement, the electric field strength, the free charge density, the free surface charge density on the external surface and that on the interface; $b_i, \sigma_{ij}, \hat{\sigma}_{ij}, u_i, \varepsilon_{ij}, T_i$ are the body force density, the stress tensor, the Maxwell stress tensor, the displacement, the strain tensor and the boundary traction on the external surface; n_j is the surface normal. To distinguish the variables in the environment from those in the film, they are denoted by superscript "env". In the domain defined by the oxide film, the local quasi-electrostatic and stress equilibrium are given by

$$D_{i,i} = q_e, \tag{1a}$$

$$\sigma_{ij,j} + \hat{\sigma}_{ij,j} + b_i = 0, \tag{1b}$$

where

$$\hat{\sigma}_{ij} = \epsilon_0 E_i E_j - \frac{1}{2}\epsilon_0 E_k E_k \delta_{ij}, \tag{2}$$

and ϵ_0 denotes the permittivity at the state with zero strain. The gradient relations are

$$E_i = -\phi_{,i}, \tag{3a}$$

$$\varepsilon_{ij} = \frac{1}{2}(u_{i,j} + u_{j,i}). \tag{3b}$$

On the external surface of the film, the boundary conditions are

$$D_j n_j = -w_e, \tag{4a}$$

$$(\sigma_{ji} + \hat{\sigma}_{ji}) n_j = T_i. \tag{4b}$$

We assume that the internal stresses and the body force in the environment are negligible. Then, the local equations in the environment become

$$D_i^{env}{}_{,i} = q_e^{env}, \tag{5}$$

$$E_i^{env} = -\phi^{env}{}_{,i}, \tag{6}$$

and the external boundary condition reduces to

$$D_j^{env} n_j^{env} = -w_e^{env}. \tag{7}$$

Across the film–environment interface, where $n_j^{env} = -n_j$, the following jump conditions exist,

$$D_j n_j + w_e^{int} = D_j^{env} n_j, \tag{8a}$$

$$\phi = \phi^{env}, \tag{8b}$$

$$(\sigma_{ji} + \hat{\sigma}_{ji}) n_j = (\sigma_{ji}^{env} + \hat{\sigma}_{ji}^{env}) n_j \approx 0. \tag{8c}$$

The equations above need to be augmented with the constitutive relations. The film is assumed to be homogeneous isotropic elastic and electrostrictive, and its isothermal electric Gibbs free energy can be expanded as (Kuang, 2009)

$$g = \frac{1}{2} C_{ijkl} \varepsilon_{ji} \varepsilon_{lk} - \frac{1}{2} \epsilon_{kl} E_k E_l - \frac{1}{2} l_{ijkl} E_i E_j \varepsilon_{lk} + \ldots, \tag{9}$$

where $C_{ijkl}, \epsilon_{kl}, l_{ijkl}$ are the material coefficients,

$$C_{ijkl} = G(\delta_{ik}\delta_{jl} + \delta_{il}\delta_{jk}) + \lambda \delta_{ij}\delta_{kl}, \tag{10a}$$

$$\epsilon_{kl} = \epsilon_0 \delta_{kl}, \tag{10b}$$

$$l_{ijkl} = \frac{1}{2} a_1 (\delta_{ik}\delta_{jl} + \delta_{il}\delta_{jk}) + a_2 \delta_{ij}\delta_{kl}. \tag{10c}$$

a_1 and a_2 are two independent electrostrictive coefficients. G and λ are the Lamé constants, which can be written as functions of Young's modulus E and Poisson ratio v, $G = E/[2(1+v)]$ and $\lambda = Ev/[(1+v)(1-2v)]$. The constitutive relations of the film are then given by

$$\sigma_{kl} = \frac{\partial g}{\partial \varepsilon_{lk}} = 2G\varepsilon_{kl} + \lambda \varepsilon_{ii}\delta_{kl} - \frac{1}{2}(a_1 E_k E_l + a_2 E_i E_i \delta_{kl}), \tag{11}$$

$$D_k = -\frac{\partial g}{\partial E_k} = (\epsilon_0 \delta_{kl} + a_1 \varepsilon_{kl} + a_2 \varepsilon_{jj}\delta_{kl}) E_l. \tag{12}$$

For the environment with negligible internal stresses, the isothermal Gibbs free energy and constitutive relation are

$$g^{env} = -\tfrac{1}{2}\epsilon_0^{env} E_k^{env} E_k^{env} \tag{13}$$

and

$$D_k^{env} = -\frac{\partial g^{env}}{\partial E_k^{env}} = \epsilon_0^{env} E_k^{env}. \tag{14}$$

Step 2. *Determination of TDF*: The TDF at the interface corresponding to the above governing equations, $\mathcal{F}$, can be computed as

$$\mathcal{F} = -\gamma\kappa - \mu - \mathbf{F}, \tag{15}$$

where $\mathbf{F}$ denotes the electromechanical energy density change at the interface. In terms of electric and stress field variables, when the interface stress vanishes, the expression of the isothermal TDF (Eq. (69)) at a moving interface in quasi-electrostatic thermoelastic continua reduces to

$$\mathbf{F} = (g + n_k E_k D_j n_j) - (g^{env} + n_k E_k^{env} D_j^{env} n_j). \tag{16}$$

The first two terms in Eq. (15) account for the variations of the surface energy and chemical energy in the system (Suo, 1997; Yu and Suo, 2000; Liang and Suo, 2001; Prevost et al., 2001), where γ is the surface energy per unit area (i.e., surface tension) of the interface, κ is twice the mean curvature of the interface, and μ is the chemical potential gained per unit volume increase of the oxide film.

Step 3. *Updating of the instantaneous profile*: The moving speed of the interface V_n is a function of $\mathcal{F}$. As a first order approximation, a linear relation is adopted (Suo, 1997; Yu and Suo, 2000; Liang and Suo, 2001; Prevost et al., 2001),

$$V_n = L\mathcal{F}, \tag{17}$$

where L denotes the interface mobility. The entropy inequality (Eq. (60f)) requires the interface to move in the direction that increases the total entropy in the system, $L > 0$. The explicit forms of L for various problems can be found in the literature (Suo, 1997; Yu and Suo, 2000; Liang and Suo, 2001; Prevost et al., 2001). For a small time increment, the instantaneous profile of the film is updated by using Eq. (17).

3. Analytical solution

This section presents analytical solutions for a perfectly flat film and for a flat film whose surface is perturbed in the form of a small amplitude undulation. In order to shed light on the breakdown phenomena, we make two assumptions about the electric field and the internal stress for the perturbed shape example that enable us to derive analytical solutions of the film's morphological evolution and its internal stress distribution. The first assumption is that the electric field is uniform, and the second is that the stress that is applied in the far-field of the film can be prescribed as the stress that develops in the flat film that is rigidly connected to the substrate. These assumptions result in an uncoupling of the electric and mechanical equations, and are consistent with the linearized problems treated in this paper. The fully coupled problem requires a computational framework that is beyond the scope of this paper, and will be the subject of future applications of the developed theory.

The film's profile is described in a Cartesian coordinate system x_i. As shown in Fig. 1a, at time t the oxide thin film occupies the region, $-h_0(t) \le x_3 \le \Delta h(x_1,x_2;t)$, where $h_0(t)$ is the average film thickness and $\Delta h(x_1,x_2;t)$ is the surface roughness. The summation accounts for the instantaneous film thickness $h(x_1, x_2; t)$,

$$h(x_1,x_2;t) = h_0(t) + \Delta h(x_1,x_2;t). \tag{18}$$

With $\Delta h(x_1,x_2;t) = 0$, Eq. (18) indicates a perfectly flat film. The surface roughness can be decomposed into a series of Fourier wavevectors. To first order the surface profile is approximated as (Fig. 1b),

$$\Delta h(x_1;t) = a(t)\cos\omega x_1, \tag{19}$$

where $a(t)$ is the instantaneous wave amplitude and ω is the perturbation wavenumber. This mathematical representation could account for an oxide film with periodic indents. A linear perturbation analysis is performed that corresponds to indents with $\omega a \ll 1$. Assuming that no electric field is imposed on the environment ($E_i^{env}=0, i=1,2,3$), then no contribution to the TDF at the film–environment interface is made by the environment. A constant electric field strength E_3 is assumed as a first approximation in the film ($E_1=E_2=0$). Electromechanical stresses arise in the film as a result of metal-film mismatch. These affect the TDF and lead to changes in the thickness and shape of the film. The solution procedure elaborated in Section 2 is followed next to determine the morphological changes of an initially perfectly flat film and of a film with sinusoidal morphology (Fig. 1b).

3.1. Flat film

The strain, stress, electric displacement, energy functions and TDF of a perfectly flat film ($n_1=n_2=0, n_3=1$) are denoted with superscript "0". Body forces and free charge are absent in the film, and its in-plane dimensions are considered large enough so that edge effects can be ignored. The metal substrate is considered infinitely thick and is regarded as rigid and perfectly bonded to the film. Therefore the in-plane strain $\varepsilon_{11}^0 = \varepsilon_{12}^0 = \varepsilon_{22}^0 = 0$. With these assumptions, application of the equations in STEP 1 provides

$$\sigma_{33}^0 = -\epsilon_0 E_3^2/2, \quad \sigma_{31}^0 = \sigma_{32}^0 = \sigma_{12}^0 = 0, \quad \sigma_{11}^0 = \sigma_{22}^0 = \left[\frac{\lambda(a_1+a_2-\epsilon_0)}{2(2G+\lambda)} - \frac{a_2}{2}\right]E_3^2,$$

$$\varepsilon_{31}^0 = \varepsilon_{32}^0 = 0, \quad \varepsilon_{33}^0 = \frac{(a_1+a_2-\epsilon_0)E_3^2}{2(2G+\lambda)},$$

$$D_1^0 = D_2^0 = 0, \quad D_3^0 = (\epsilon_0 + a_1\varepsilon_{33}^0 + a_2\varepsilon_{33}^0)E_3. \tag{20a–g}$$

Substitution of the field variables listed above into Eq. (16) in STEP 2, the electromechanical energy density change at the interface is found

$$\mathsf{F}^0 = \frac{\epsilon_0 E_3^2}{2} + \alpha\left(\frac{\epsilon_0 E_3^2}{2}\right)^2, \tag{21}$$

where α is a utility constant comprised of elastic and electrostrictive material parameters. The explicit expression of α is given in Appendix C, and the normalized curves for α are depicted in Fig. 3. Since the film is perfectly flat (i.e., $\kappa = 0$), the TDF is dominated by the chemical energy density and electromechanical energy density, $\mathcal{F}^0 = -\mu - \mathsf{F}^0$. According to the kinetic law in STEP 3, the film will remain flat and its instantaneous thickness is

$$h_0(t) = H_0 - L\left[\mu + \frac{\epsilon_0 E_3^2}{2} + \alpha\left(\frac{\epsilon_0 E_3^2}{2}\right)^2\right]t, \tag{22}$$

where H_0 is the initial average thickness of the film. The implications of this result are discussed in the next section.

3.2. Film with sinusoidal surface

The profile evolution of a film with periodical undulations is considered next. An analytical solution results from the following ansatz. The film is perfectly restrained by the metal substrate in the x_2 direction, so that $\varepsilon_{22} = 0$. The rigid constraint

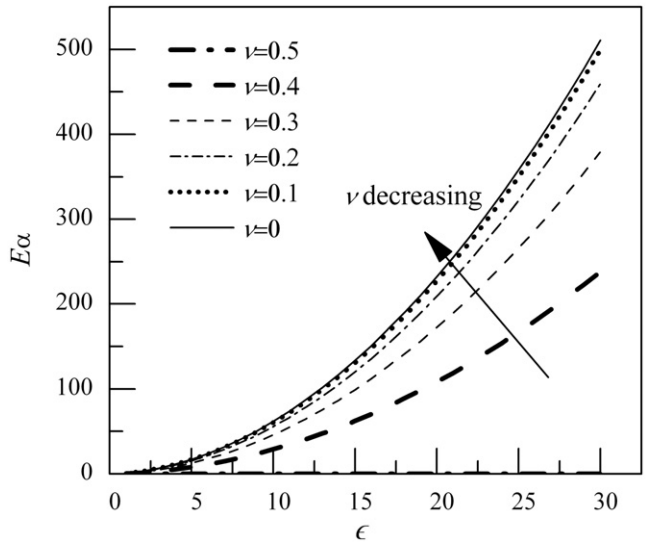

Fig. 3. Combined material parameter α as functions of Poisson ratio ν and dielectric constant ϵ.

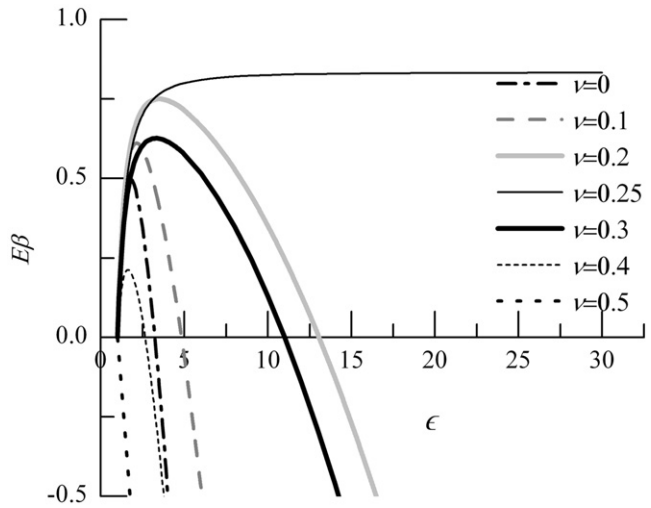

Fig. 4. Combined material parameter β as functions of Poisson ratio ν and dielectric constant ϵ.

induced by the substrate in the x_1 direction is approximated by subjecting the film to a far-field mismatch stress along direction x_1, whose magnitude equals the mismatch stress originating in the flat film, σ_{11}^0. In addition, the shear strains ε_{12} and ε_{32} are assumed to be zero, rendering the problem of the plane-strain type. The detailed derivation for the stress field σ_{ij} and strain field ε_{ij} is provided in Appendix B. Substitution of the field variables into Eq. (16) and taking the leading order of amplitude a leads to

$$\mathsf{F} = \mathsf{F}^0 + \Delta\mathsf{F}, \tag{23}$$

where $\Delta\mathsf{F}$ is the interfacial electromechanical energy density change associated with introducing the sinusoidal surface,

$$\Delta\mathsf{F} = -a\omega\beta\chi\left(\frac{\epsilon_0 E_3^2}{2}\right)^2 \cos\omega x_1. \tag{24}$$

β is another utility constant and χ is the (ωh_0)−dependent coefficient. Both explicit forms are defined in Appendix C. The normalized curves for β are plotted in Fig. 4, and χ is shown in Fig. 5. It is important to note that β determines whether the amplitude of the perturbation approaches the initial thickness of the film and leads to passive exposure of the substrate to the environment. Specifically, as clarified in Section 4, if $\beta \le 0$ the film remains flat, while if $\beta > 0$ the substrate can be exposed. The normal interfacial migration velocity becomes $V_n = h_{,t}[1+(h_{,1})^2]^{-1/2} = h_{,t}[1+(a\omega\sin\omega x_1)^2]^{-1/2}$. Since $\omega a \ll 1$, it reduces to

$$V_n = \frac{\partial h}{\partial t} = \frac{dh_0}{dt} + \frac{da}{dt}\cos\omega x_1. \tag{25}$$

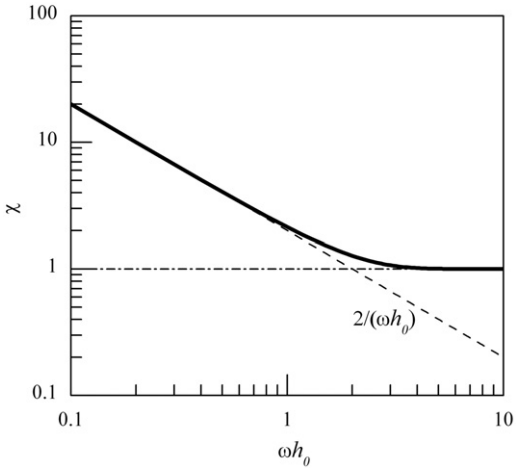

Fig. 5. Morphology coefficient χ as a function of (ωh_0).

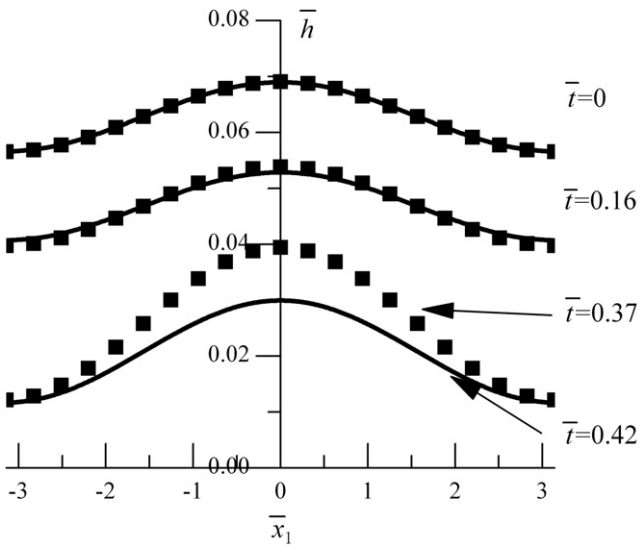

Fig. 6. Illustrative examples of profile evolution. $\bar{x}_1$ and $\bar{h}$ are on different scales. Solid lines and dotted lines are for case $*$ and case $**$ in Table 1, respectively.

The curvature of the sinusoidal surface is also simplified as $\kappa = -h_{,11}[1+(h_{,1})^2]^{-3/2} \approx -h_{,11} = a\omega^2 \cos\omega x_1$. Thus the TDF in STEP 2 is determined as $\mathcal{F} = -\mu - \kappa\gamma - \mathbb{F} = \mathcal{F}^0 + a(-\omega^2\gamma + \omega\beta\chi(\epsilon_0 E_3^2/2)^2)\cos\omega x_1$. Based on the kinetic law in STEP 3, a set of equations to predict the surface movements is obtained. The evolution of film average thickness can be depicted by Eq. (22). The amplitude change can then be calculated from

$$\Delta h(x_1;t) = a_0 \exp\left(L\left(-\omega^2\gamma + \omega\beta\chi\left(\frac{\epsilon_0 E_3^2}{2}\right)^2\right)t\right)\cos\omega x_1, \tag{26}$$

where a_0 is the initial amplitude of the wavy film–solution interface. The form of the equations above are similar to the surface migration profiles solved by Srolovitz (1989) and others (Yu and Suo, 2000; Yang, 2006), except that the results obtained here include the effects of electrostriction and express the instantaneous profile explicitly in terms of the applied electric field strength and utility (combined material) constants. The implications of the result is discussed next.

4. Results and discussion

The analytical solutions derived in Section 3 enable us to capture the evolution of the morphologies of the film and evaluate the level of internal stresses for given conditions in experiments and in practice. When the amplitude is small, the time evolution of one surface wave mode is independent of that of the other. The film's surface profile then can be treated as a

linear combination of several primary in-plane orthogonal wave modes, and its roughness can be represented as

$$\Delta h(x_1;t)=\sum_{k=1}^{n}\Delta h_k=\sum_{k=1}^{n}\exp\left(L\left(-(k\omega)^2\gamma+(k\omega)\beta\chi_k\left(\frac{\epsilon_0E_3^2}{2}\right)^2\right)t\right)(a_k\cos k\omega x_1+b_k\sin k\omega x_1), \tag{27}$$

where a_k, b_k indicate the wave amplitudes for mode k. χ_k is the morphology factor for wavenumber $k\omega$. Based on Eqs. (22) and (27), we carry out a normalization procedure, discuss the variables that control the corrosion resistance and propose experimental measurement method for film's properties and functional life.

4.1. Normalization

For most oxide films, $\alpha>0$ with a unit of 1/stress, based on which we introduce a set of normalized parameters: the chemical energy density, $\overline{\mu}=\alpha\mu$; the electrostatic energy density, $\overline{U}_E=\alpha(\epsilon_0E_3^2/2)$; the minimum wavenumber, $\overline{\omega}=\alpha\gamma\omega$; the instantaneous thickness, $\overline{h}=\omega h$; the instantaneous averaged thickness, $\overline{h}_0=\omega h_0$; the initial thickness, $\overline{H}_0=\omega H_0$; the instantaneous surface roughness, $\overline{\Delta h}=\omega\Delta h$; the initial amplitudes, $\overline{a}_k=\omega a_k$ and $\overline{b}_k=\omega b_k$; the time, $\overline{t}=L\gamma\omega^2t$; the coordinate, $\overline{x}_i=\omega x_i$. Eqs. (22) and (27) can then be simplified to

$$\overline{h}_0(\overline{t})=\overline{H}_0-\frac{\overline{t}}{\overline{\omega}}(\overline{\mu}+\overline{U}_E+\overline{U}_E^2)=\overline{H}_0+\overline{\xi}\overline{t} \tag{28}$$

and

$$\begin{aligned}\overline{\Delta h}(\overline{x}_1;\overline{t})=&\sum_{k=1}^{n}\overline{\Delta h}_k=\sum_{k=1}^{n}\exp\left(\left(-k^2+\frac{k\beta\overline{U}_E^2}{\alpha\overline{\omega}}\chi_k\right)\overline{t}\right)(\overline{a}_k\cos k\overline{x}_1\\&+\overline{b}_k\sin k\overline{x}_1)=\sum_{k=1}^{n}\exp(\overline{\zeta}_k\overline{t})(\overline{a}_k\cos k\overline{x}_1+\overline{b}_k\sin k\overline{x}_1),\end{aligned} \tag{29}$$

where $\overline{\xi}$ and $\overline{\zeta}_k$ are defined as the normalized growth rates of film average thickness and film roughness, respectively. The surface movement of a perfectly flat film can also be described by Eqs. (28) and (29) by setting $\overline{a}_k=\overline{b}_k=0$. Therefore, without loss of generality, we can first determine $\overline{h}_0$ using Eq. (28), and then substitute its value into Eq. (29) to calculate $\overline{\Delta h}$, and in turn calculate the normalized instantaneous film thickness through

$$\overline{h}=\overline{h}_0(\overline{t})+\overline{\Delta h}(\overline{x}_1;\overline{t}). \tag{30}$$

4.2. Qualitative analysis for the breakdown mechanism

The variation of $\overline{h}_0$ (Eq. (28)) is apparent. For a negative change in chemical potential due to an increased volume of oxide film, $\overline{\mu}<0$, there exists a critical electrostatic energy density,

$$\overline{U}_E^{cr}=\frac{-1+\sqrt{1-4\overline{\mu}}}{2}, \tag{31}$$

at which the normalized growth rate $\overline{\xi}$ is zero. For $\overline{U}_E>\overline{U}_E^{cr}$ ($\overline{U}_E<\overline{U}_E^{cr}$), $\overline{\xi}<0$ ($\overline{\xi}>0$) and $\overline{h}_0$ continues decreasing (growing).

The evolution of $\overline{\Delta h}_k$ (Eq. (29)), however, is more complex because of its dependence on the instantaneous χ_k. Simplified forms for χ_k can be derived for infinite-thick and ultra-thin films.

For an infinitely-thick film, $k\overline{h}_0\gg1$, and $\chi_k\approx1$ (Fig. 5). Hence, the growth rate of surface roughness is reduced to

$$\overline{\zeta}_k=k^2(-1+\overline{\iota}_k), \tag{32}$$

where $\overline{\iota}_k=\beta\overline{U}_E^2/(\alpha k\overline{\omega})$. When $\overline{\iota}_k=1$, the amplitude of the surface wave remains constant. For $\overline{\iota}_k>1$ ($\overline{\iota}_k<1$), $\overline{\Delta h}_k$ monotonically increases (decays). The time evolution of the very thick film could also be considered as the evolution of a finite-thick film whose surface is the shape of very shallow waves. This corresponds to the early stage of the morphological evolution. Unless the stress concentration associated with the shallow waves is significant, then this limiting configuration is not relevant to pitting corrosion.

This study assumes that pitting is a result of surface migration only and focuses on the time evolution of very thin films with deep indents, which could be regarded as the precursors to dielectric breakdown or substrate exposure. For a finite-thick film with $k\overline{h}_0<1$, and a Fourier expansion leads to $\chi_k\approx2/(k\overline{h}_0)$ (Fig. 5). Therefore, the growth rate is time-dependent,

$$\overline{\zeta}_k=k^2\left(-1+\frac{2\overline{\iota}_k}{k\overline{h}_0}\right)=k^2\left(-1+\frac{2\overline{\iota}_k}{k(\overline{H}_0+\overline{\xi}\overline{t})}\right). \tag{33}$$

Various trends are exhibited by $\overline{\Delta h}_k$: if $\overline{\iota}_k\le0$ (i.e., $\beta\le0$), $\overline{\Delta h}_k$ monotonically decreases; if $0<\overline{\iota}_k<k\overline{H}_0/2$ and $\overline{U}_E=\overline{U}_E^{cr}$, $\overline{\Delta h}_k$ monotonically decreases; if $\overline{\iota}_k=k\overline{H}_0/2$ and $\overline{U}_E=\overline{U}_E^{cr}$, $\overline{\Delta h}_k$ is invariant; if $\overline{\iota}_k>k\overline{H}_0/2$ and $\overline{U}_E=\overline{U}_E^{cr}$, $\overline{\Delta h}_k$ monotonically increases; if $\overline{\iota}_k\ge k\overline{H}_0/2$ and $\overline{U}_E>\overline{U}_E^{cr}$, $\overline{\Delta h}_k$ monotonically increases; if $0<\overline{\iota}_k<k\overline{H}_0/2$ and $\overline{U}_E>\overline{U}_E^{cr}$, $\overline{\Delta h}_k$ first decreases then

Table 1
The evolution of film average height and roughness. The bottom row and rightmost column are conducive to film breakdown. Numerical examples for $*$ and $**$ are shown in Fig. 6.

Case	$\overline{h}_0$	$\overline{\Delta h}_k$			
		$\overline{\tau}_k \le 0$	$0 < \overline{\tau}_k < \frac{k\overline{H}_0}{2}$	$\overline{\tau}_k = \frac{k\overline{H}_0}{2}$	$\overline{\tau}_k > \frac{k\overline{H}_0}{2}$
$\overline{U}_E < \overline{U}_E^{cr}$	$\uparrow$	$\downarrow$	$\downarrow$	$\downarrow$	$\uparrow$ then $\downarrow$
$\overline{U}_E = \overline{U}_E^{cr}$	Unchange	$\downarrow$	$\downarrow$	Unchange	$\uparrow$
$\overline{U}_E > \overline{U}_E^{cr}$	$\downarrow$	$\downarrow$	$\downarrow$ then $\uparrow^{(*)}$	$\uparrow$	$\uparrow^{(**)}$

increases; if $\overline{\tau}_k > k\overline{H}_0/2$ and $\overline{U}_E < \overline{U}_E^{cr}$, $\overline{\Delta h}_k$ first increases then decreases; if $0 < \overline{\tau}_k \le k\overline{H}_0/2$ and $\overline{U}_E < \overline{U}_E^{cr}$, $\overline{\Delta h}_k$ monotonically decreases.

The evolutions of $\overline{h}_0$ and $\overline{\Delta h}_k$ for an ultra-thin film, summarized in Table 1, suggest that oxide films could break down if either $\overline{U}_E > \overline{U}_E^{cr}$ or $\overline{\tau}_k > k\overline{H}_0/2$. The results are intuitive; the former is associated with complete depletion of the film, and the latter with wearing away of the film in periodic locations. In experimental measurements (Martin et al., 2007, 2009), the two criteria may be associated with the breakdown potentials for transpassive dissolution and pitting corrosion. Failure can be mitigated if $\overline{U}_E \le \overline{U}_E^{cr}$ and $\overline{\tau}_k \le \overline{\tau}_1 \le \overline{H}_0/2$. For given conditions in real practice, these two critical conditions together could determine the breakdown electric field strength, which is written explicitly as

$$({}_1E_3^{cr})^2 = \frac{-1+\sqrt{1-4\alpha\mu}}{\alpha\epsilon_0}, \tag{34a}$$

$$({}_2E_3^{cr})^2 = \left(\frac{2\omega^2\gamma H_0}{\beta\epsilon_0^2}\right)^{1/2}, \tag{34b}$$

and

$$(E_3^{cr})^2 = \min\{({}_1E_3^{cr})^2, ({}_2E_3^{cr})^2\}. \tag{35}$$

From the perspective of film design, one can first obtain the critical electric potential field by Eq. (34a) for given properties of film and corrosive environment, then estimate the allowable minimum film thickness in terms of minimum wavenumber ω, a measure of critical thickness by Eq. (34b) as

$$H_0^{cr} = \frac{\beta}{2\omega^2\gamma}\left(\frac{-1+\sqrt{1-4\alpha\mu}}{\alpha}\right)^2. \tag{36}$$

Eq. (36) indicates that a higher density of undulations, associated with increased surface energy promoting smoothing of the surface, demands a thinner initial average film thickness to avoid localized pitting.

The results prove that reduction of film thickness followed by either dielectric breakdown or exposure of the substrate to the environment, is possible. Unfortunately, experimentally measured values of the parameters, γ, μ, α, and β, are not available, so that the results presented above can be used only for qualitative insights. However, an experimental procedure that can in principle be used to measure them is proposed next.

4.3. Experimental measurement method

The instantaneous shape of the film's surface (Eq. (27)) can also be expanded as complex Fourier series,

$$h(x_1,t) = \sum_{k=-\infty}^{\infty} q_k(k\omega,t)\exp(jk\omega x_1), \tag{37}$$

where the complex wave amplitude is defined by

$$q_0(0,t) = h_0(t),$$

$$q_k(k\omega,t) = \frac{1}{2}(a_k - jb_k)\exp\left(L\left(-(k\omega)^2\gamma + (k\omega)\beta\chi_k\left(\frac{\epsilon_0 E_3^2}{2}\right)^2\right)t\right),$$

$$q_{-k}(-k\omega,t) = \frac{1}{2}(a_k + jb_k)\exp\left(L\left(-(k\omega)^2\gamma + (k\omega)\beta\chi_k\left(\frac{\epsilon_0 E_3^2}{2}\right)^2\right)t\right). \tag{38a–c}$$

An atomic force microscope (AFM) can be used to scan and quantify the surface topologies at initial time and current time, $h(x_1; 0)$ and $h(x_1; t)$, respectively. Then, the complex wave amplitude can be recovered by the Fourier transform,

$$q_k(k\omega,t) = \int_{-\infty}^{\infty} h(x_1;t)\exp(-jk\omega x_1)\, dx_1. \tag{39}$$

According to Eq. (38), the ratio of two complex wave amplitudes is a function of the film's properties,

$$\frac{1}{t}\ln\frac{q_k(k\omega,t)}{q_k(k\omega,0)} = L\left(-(k\omega)^2\gamma + (k\omega)\beta\chi_k\left(\frac{\epsilon_0 E_3^2}{2}\right)^2\right). \tag{40}$$

The film's elastic constants, E and ν, are assumed to be known from other measurements. The utility constants, α and β, can be expressed in terms of ϵ_0 (Appendix C). The four unknown properties, L, μ, γ and ϵ_0, can then be evaluated by Eqs. (22) and (40) for two different values of E_3. Then, the functional life of the coating, or the critical electrical field strength (Eq. (34a)) and the minimum initial thickness (Eq. (36)) are found.

4.4. Numerical examples

The two illustrative cases defined in Table 1, $*$ and $**$, are selected to illustrate the shape change of a finite-thick oxide film with one cosine wave component. The normalized initial thickness, the normalized initial amplitude and the normalized growth rates of the average thickness are chosen to be equal, $\overline{H}_0 = 0.0628$, $\overline{a}_1 = 0.00628$, and $\overline{\xi} = -0.1$. Then $\overline{\imath}_1 = 0.02 < \overline{H}_0/2$ for $*$ and have $\overline{\imath}_1 = 0.04 > \overline{H}_0/2$ for $**$. In both cases, the film is depleted in places, however, pitting corrosion occurs "later" for $*$ than $**$. It is also apparent that the pitting corrosion will occur "faster" for larger $\overline{a}_k$, $\overline{b}_k$ and smaller $\overline{\xi}$ and $\overline{H}_0$. The real time scale can be found by $t = \overline{t}/(L\gamma\omega^2)$. We speculate that the normalized parameters or the time mapping vary in an experiment (Martin et al., 2007, 2009), and therefore significant improvements in corrosion resistance can be achieved.

5. Conclusion

A continuum framework was presented to analyze the shape changes of protective oxide films subjected to electrostrictive forces and a corrosive environment. Analytical solutions were found for oxide films subjected to a constant and uniform electric strength. Instantaneous film profiles were obtained as functions of normalized control variables. The results showed that under a critical combination of electric field strength, initial average thickness and density of surface roughness, the finite-thick film can be thinned enough to undergo dielectric breakdown, or be partly depleted that leads to substrate pitting corrosions. The time mapping and the normalized initial average thickness, initial wave amplitudes, growth rates for average thickness and roughness, $\overline{H}_0$, $\overline{a}_k$, $\overline{b}_k$, $\overline{\xi}$, $\overline{\imath}_k$, are the most significant in terms of corrosion resistance. The properties of the coating can be measured by the proposed experimental method, by which both the critical combination and the corrosion resistance can be estimated. The formulation described in the paper can be generalized to include the effects of prestress, flexoelectric stress, stress concentration, and mechanical failure using the finite element method. In principle the model presented here can be used to design an immortal passivating film.

Acknowledgement

The authors acknowledge support from the James L. Record Chair in the department of Civil Engineering at University of Minnesota.

Appendix A. TDF on a singular discontinuity in thermoelectroelastic continua in the presence of quasi-electrostatic field

The TDF acting on a singular discontinuity associated with numerous physical problems has been widely studied. Abeyaratne and Knowles (1990) derived the driving traction for thermoelastic solids; Jiang (1994) considered the presence of both electromagnetic and elastic fields, but omitted electromagnetic forces in the linear and angular momentum; James (2002) established a more comprehensive formulation of the TDF in a shape memory alloy by considering magnetostatic (magnetization and demagnetization) and elastic fields. In this section, following the same procedure in Abeyaratne and Knowles (1990) and Jiang (1994), the TDF at a moving singular surface in quasi-electrostatic thermoelastic continua is derived.

A.1. Bodies, deformations and motions

Consider a system $\mathfrak{S}$ comprised of the two thermoelectroelastic materials shown in Fig. 2. At time $t=0$, the two materials that are separated by a singular surface S_0 occupying region $D_0 - S_0$ (i.e., $D_0^+ \cup D_0^-$), which is referred as the reference configuration. X_I denotes the referential (or particle) position of $\mathfrak{S}$. At current time t, the interface is denoted by S_t, and the current configuration $D_t - S_t$ (i.e., $D_t^+ \cup D_t^-$) of $\mathfrak{S}$ can be described by an invertible mapping $x_i = \varkappa_i(X_K,t)$. Then,

$$F_{ij} = \frac{\partial \varkappa_i(X_K,t)}{\partial X_J}, \quad J = det(F_{ij}), \quad F_{Ij}^{-1} = \frac{\partial \varkappa_I^{-1}(x_k,t)}{\partial x_j} \tag{41a, b, c}$$

represent the deformation gradient, its Jacobian and its inverse matrix. The particle velocity is defined as

$$v_i = \frac{\partial \varkappa_i(X_K,t)}{\partial t}. \tag{42}$$

The material time derivative operator is

$$\dot{(\,)} = \frac{D}{Dt} = \frac{\partial}{\partial t} + v_k \frac{\partial}{\partial x_k}. \tag{43}$$

If the singular discontinuity surface moves with a speed v_k^s in the current state (Fig. 2), the corresponding velocities of both its sides in the reference state are

$$V_J^{\pm} = (v_k^s - v_k^{\pm})(F_{Jk}^{-1})^{\pm}. \tag{44}$$

The smoothness requirement of the deformation fields, $V_J^+ = V_J^- = V_J$ (or $\|V_J\| = 0$), demands that (Abeyaratne and Knowles, 1990)

$$\|F_{kJ}\| L_J = 0, \quad \|v_k\| = -\|F_{kJ}\| V_J = -\|F_{kJ}\| V_n N_J, \tag{45a, b}$$

where L_J is any vector tangent to the singular surface. N_J is the surface normal in reference state, and V_n is the normal component of V_J (i.e., $V_n = V_J N_J$). $\|(.)\|$ represents the jump $(.)^+ - (.)^-$.

A.2. Global balance and energy laws

Define a set of true field variables in the current state: ϕ, d_i, e_i, q_e, w_e represent the electric potential, the electric displacement, the electric field strength, the free charge density, and the free surface charge density; on the external surface ∂D_t of $\Im$ at time t, $w_e = -d_i n_i$, where n_i is the surface normal; $\rho, f_i, \sigma_{ij}, \hat{\sigma}_{ij}$ are the mass density, the body force per unit mass, the stress tensor and the Maxwell stress tensor; $t_i = (\sigma_{ji} + \hat{\sigma}_{ji}) n_j$ denotes the boundary traction on ∂D_t; u^p, $\dot{r}$, q_i, Γ, η, θ are the internal energy density per unit mass, the heat supply rate per unit mass, the heat flux, the total rate of entropy production, the entropy density per unit mass, and the absolute temperature. These variables satisfy the quasi-electrostatic Gauss and Faraday laws (Eringen and Maugin, 1990; Harper, 1999),

$$\int_{\partial D_t} d_i n_i \, dA = \int_{D_t - S_t} q_e \, dV + \int_{S_t} w_e \, dA, \tag{46a}$$

$$\oint_{\partial C_t} e_i \, dx_i = 0, \tag{46b}$$

the mass conservation law,

$$\int_{D_t - S_t} \rho \, dV = 0, \tag{47}$$

balance laws of linear and angular momentum (Harper, 1999),

$$\int_{D_t - S_t} \rho f_i \, dV + \int_{\partial D_t} t_i \, dA = \frac{D}{Dt} \int_{D_t - S_t} \rho v_i \, dV, \tag{48a}$$

$$\int_{D_t - S_t} \varepsilon_{ijk} x_j (\rho f_k) \, dV + \int_{\partial D_t} \varepsilon_{ijk} x_j t_k \, dA = \frac{D}{Dt} \int_{D_t - S_t} \varepsilon_{ijk} x_j (\rho v_k) \, dV, \tag{48b}$$

the energy conservation law (McMeeking et al., 2007),

$$\begin{aligned} \frac{D}{Dt} \int_{D_t - S_t} \left(\frac{1}{2} \rho v_i v_i + \rho u^p \right) dV = & \int_{D_t - S_t} \rho \dot{r} \, dV - \int_{\partial D_t} q_i n_i \, dA + \int_{D_t - S_t} \rho f_i v_i \, dV + \int_{\partial D_t} t_i v_i \, dA \\ & - \int_{D_t - S_t} \dot{\phi} q_e \, dV - \int_{\partial D_t} \dot{\phi} w_e \, dA - \int_{S_t} \|\dot{\phi} d_i\| n_i \, dA, \end{aligned} \tag{49}$$

and the entropy inequality law (Abeyaratne and Knowles, 1990; Jiang, 1994; Harper, 1999),

$$\Gamma = \frac{D}{Dt} \int_{D_t - S_t} \rho \eta \, dV + \int_{\partial D_t} \frac{q_i n_i}{\theta} \, dA - \int_{D_t - S_t} \frac{\rho \dot{r}}{\theta} \, dV \geq 0, \tag{50}$$

where C_t is any surface in the current configuration and ∂C_t is its line circuit (depicted in Fig. 2). The following equalities apply to any infinitesimal volume, surface, and line elements in the reference configuration and those in the current configuration, (Eringen and Maugin, 1990; Harper, 1999),

$$dV = J \, dV_0, \quad n_i \, dA = J F_{Ji}^{-1} N_J \, dA_0, \quad dx_i = F_{iJ} \, dX_J. \tag{51a, b, c}$$

By applying Eq. (51) to Eqs. (46)–(50), the corresponding physical quantities in the reference state denoted by capital letters are found,

$$D_J = JF_{Ji}^{-1} d_i, \quad E_J = e_i F_{iJ}, \quad Q_e = q_e J,$$

$$\varrho = \rho J, \quad \Sigma_{Ji} = JF_{Jk}^{-1}\sigma_{ki}, \quad \hat{\Sigma}_{Ji} = JF_{Jk}^{-1}\hat{\sigma}_{ki}, \quad Q_J = JF_{Ji}^{-1} q_i, \tag{52a–g}$$

on external surface ∂D_0 of $\mathfrak{S}$ at initial time,

$$W_e = -D_J N_J, \quad T_i = (\Sigma_{Ji} + \hat{\Sigma}_{Ji}) N_J. \tag{53a, b}$$

The physical variables, ϕ, f_i, u^p, $\dot{r}$, Γ, η, θ, are the same in the current and reference configurations. Eqs. (46)–(50) in the reference state are written as

$$\int_{\partial D_0} D_J N_J \, dA_0 = \int_{D_0 - S_0} Q_e \, dV_0 + \int_{S_0} W_e \, dA_0, \tag{54a}$$

$$\oint_{\partial C_0} E_J \, dX_J = 0, \tag{54b}$$

$$\frac{D}{Dt}\int_{D_0 - S_0} \varrho \, dV_0 = 0, \tag{54c}$$

$$\int_{D_0 - S_0} \varrho f_i \, dV_0 + \int_{\partial D_0} T_i \, dA_0 = \frac{D}{Dt}\int_{D_0 - S_0} \varrho v_i \, dV_0, \tag{54d}$$

$$\int_{D_0 - S_0} \varepsilon_{ijk} x_j (\varrho f_k) \, dV_0 + \int_{\partial D_0} \varepsilon_{ijk} x_j T_k \, dA_0 = \frac{D}{Dt}\int_{D_0 - S_0} \varepsilon_{ijk} x_j (\varrho v_k) \, dV_0, \tag{54e}$$

$$\begin{aligned} \frac{D}{Dt}\int_{D_0 - S_0} \left(\frac{1}{2}\varrho v_i v_i + \varrho u^p\right) dV_0 &= \int_{D_0 - S_0} \varrho \dot{r} \, dV_0 - \int_{\partial D_0} Q_J N_J \, dA_0 + \int_{D_0 - S_0} \varrho f_i v_i \, dV_0 + \int_{\partial D_0} T_i v_i \, dA_0 \\ &- \int_{D_0 - S_0} \dot{\phi} Q_e \, dV_0 - \int_{\partial D_0} \dot{\phi} W_e \, dA_0 - \int_{S_0} \|\dot{\phi} D_J\| N_J \, dA_0, \end{aligned} \tag{54f}$$

$$\Gamma = \frac{D}{Dt}\int_{D_0 - S_0} \varrho \eta \, dV_0 + \int_{\partial D_0} \frac{Q_J N_J}{\theta} \, dA_0 - \int_{D_0 - S_0} \frac{\varrho \dot{r}}{\theta} \, dV_0 \geq 0, \tag{54g}$$

where C_0 and ∂C_0 (depicted in Fig. 2) are the chosen surface and its line circuit in the reference configuration.

A.3. Generalized Green–Gauss, Reynolds transport and Stokes theorems

In the presence of the singular surface (Fig. 2), the generalized Green–Gauss theorem is (Eringen and Maugin, 1990; Harper, 1999),

$$\int_{\partial D_0} (.) N_J \, dA_0 = \int_{D_0 - S_0} (.)_{,J} \, dV_0 + \int_{S_0} \|(.)\| N_J \, dA_0, \tag{55}$$

where $(.)$ can be a vector component such as D_J or a tensor component such as Σ_{Ji}; the generalized Reynolds transport theorem takes the following form (Eringen and Maugin, 1990; Harper, 1999),

$$\frac{D}{Dt}\int_{D_0 - S_0} (.) J \, dV_0 = \int_{D_0 - S_0} \left[\frac{\partial (.)}{\partial t} + ((.) v_k)_{,k}\right] J \, dV_0 - \int_{S_0} \|(.) J\| V_n \, dA_0, \tag{56}$$

where $(.)$ can be a scalar such as ρ or a vector component such as ρv_i; the generalized Stokes theorem becomes (Eringen and Maugin, 1990; Harper, 1999)

$$\oint_{\partial C_0} E_J \, dX_J = \int_{C_0 - r_0} \varepsilon_{IJK} E_{K,J} N_I \, dA_0 + \int_{r_0} \|E_J\| \, dX_J, \tag{57}$$

where r_0 is a discontinuous line on surface C_0.

A.4. Local equations and jump conditions

Based on Eqs. (43)–(45) and (55), one obtains

$$-\int_{\partial D_0} \dot{\phi} W_e \, dA_0 - \int_{S_0} \|\dot{\phi} D_J\| N_J \, dA_0 = \int_{\partial D_0} \left(\frac{\partial \phi}{\partial t} + v_k \frac{\partial \phi}{\partial x_k}\right) D_J N_J \, dA_0 - \int_{S_0} \left\| \left(\frac{\partial \phi}{\partial t} + v_k \frac{\partial \phi}{\partial x_k}\right) D_J \right\| N_J \, dA_0$$

$$-\int_{S_0}\left\|(v_k^s-v_k)\frac{\partial\phi}{\partial x_k}D_J\right\|N_J\,dA_0=\int_{D_0-S_0}(\dot{\phi}D_J)_{,J}\,dV_0-\int_{S_0}\|\phi_{,K}D_J\|V_nN_JN_K\,dA_0. \tag{58}$$

By applying Eqs. (55)–(58) to Eq. (54), and using the postulate of localization Eringen and Maugin (1990), the local equations in D_0-S_0 read

$$D_{J,J}=Q_e, \tag{59a}$$

$$E_J=-\phi_{,J}\ \text{(i.e., } \varepsilon_{IJK}E_{K,J}=0), \tag{59b}$$

$$\left[\frac{\partial\rho}{\partial t}+(\rho v_k)_{,k}\right]J=0, \tag{59c}$$

$$\varrho\dot{v}_i=(\Sigma_{Ji}+\hat{\Sigma}_{Ji})_{,J}+\varrho f_i, \tag{59d}$$

$$F_{iK}(\Sigma_{Kj}+\hat{\Sigma}_{Kj})=(\Sigma_{jK}+\hat{\Sigma}_{jK})F_{Ki}, \tag{59e}$$

$$\varrho\dot{u^p}=\varrho\dot{r}-Q_{J,J}+(\Sigma_{Ji}+\hat{\Sigma}_{Ji})v_{i,J}-\dot{E}_JD_J, \tag{59f}$$

$$\varrho\dot{\eta}+\left(\frac{Q_J}{\theta}\right)_{,J}-\frac{\varrho\dot{r}}{\theta}\geq 0, \tag{59g}$$

and the jump conditions across S_0 read,

$$\|D_J\|N_J=W_e, \tag{60a}$$

$$\|\phi\|=0, \tag{60b}$$

$$\|\varrho\|V_n=0, \tag{60c}$$

$$\|\varrho v_i\|V_n+\|\Sigma_{Ji}+\hat{\Sigma}_{Ji}\|N_J=0, \tag{60d}$$

$$\|\tfrac{1}{2}\varrho v_iv_i+\varrho u^p\|V_n+\|(\Sigma_{Ji}+\hat{\Sigma}_{Ji})v_i\|N_J+\|E_KD_J\|V_nN_JN_K-\|Q_J\|N_J=0, \tag{60e}$$

$$\|-\varrho\eta\|V_n+\left\|\frac{Q_J}{\theta}\right\|N_J\geq 0. \tag{60f}$$

A.5. The TDF acting at the discontinuous surface

The following equality exists for two variables a and b,

$$\|ab\|=\|a\|\langle b\rangle+\langle a\rangle\|b\|, \tag{61}$$

where $\langle a\rangle$ denotes the average $\frac{1}{2}(a^++a^-)$. By utilizing this identity together with Eqs. (60d) and (45), one can easily prove (Abeyaratne and Knowles, 1990),

$$\|(\Sigma_{Ji}+\hat{\Sigma}_{Ji})v_i\|N_J=[-\|\tfrac{1}{2}\varrho v_iv_i\|-\|(\Sigma_{Ji}+\hat{\Sigma}_{Ji})F_{iK}\|N_KN_J+\tfrac{1}{2}\varrho V_n^2\|F_{iK}F_{ij}\|N_KN_J]V_n. \tag{62}$$

Hence, from Eq. (60e), we have

$$\|Q_J\|N_J=[\|\varrho u^p\|-\|(\Sigma_{Ji}+\hat{\Sigma}_{Ji})F_{iK}\|N_KN_J+\tfrac{1}{2}\varrho V_n^2\|F_{iK}F_{ij}\|N_KN_J+\|E_KD_J\|N_KN_J]V_n. \tag{63}$$

We assume that the absolute temperature is continuous across S_0, $\|\theta\|=0$. Then, the total entropy production rate (Eq. (54g)) becomes (Abeyaratne and Knowles, 1990; Jiang, 1994)

$$\Gamma=\Gamma_{loc}+\Gamma_{con}+\Gamma_{S_0}, \tag{64}$$

where Γ_{loc} represents the entropy production rate generating from local dissipation, Γ_{con} is the entropy production rate due to heat conduction, and Γ_{S_0} denotes the entropy production rate arising from moving discontinuous surface. They are written explicitly as

$$\Gamma_{loc}=\int_{D_0-S_0}\frac{\varrho\dot{\eta}\theta+Q_{J,J}-\varrho r}{\theta}dV_0, \tag{65a}$$

$$\Gamma_{con}=-\int_{D_0-S_0}\frac{Q_J\theta_{,J}}{\theta^2}dV_0, \tag{65b}$$

$$\Gamma_{S_0}=\int_{S_0}\frac{-\|\varrho\eta\theta\|V_n+\|Q_J\|N_J}{\theta}dA_0. \tag{65c}$$

Γ_{S_0} could be rewritten in terms of the TDF $\mathcal{F}$, the temperature θ and the normal velocity V_n of the moving singular surface (Abeyaratne and Knowles, 1990; Jiang, 1994), that is

$$\Gamma_{S_0} = \int_{S_0} \frac{\mathcal{F} V_n}{\theta} dA_0. \tag{66}$$

By using Eq. (63) and introducing the electric Gibbs free energy density (i.e., electric enthalpy),

$$g = \varrho u^p - \varrho \eta \theta, \tag{67}$$

we obtain the driving force acting at the singular surface,

$$\mathcal{F} = \frac{-\|\varrho \eta \theta\| V_n + \|Q_J\| N_J}{V_n} = \|g\delta_{JK} - (\Sigma_{Ji} + \hat{\Sigma}_{Ji}) F_{iK} + \frac{1}{2}\varrho V_n^2 F_{iK} F_{iJ} + E_K D_J\| N_K N_J. \tag{68}$$

This format is similar to the expression derived from a different procedure (Maugin and Trimarco, 1997). For a slow isothermal process, the interia terms in Eq. (60d) and the kinematic energy in Eq. (60e) vanish. Hence, one can easily find

$$\mathcal{F} = \|g\delta_{JK} - (\Sigma_{Ji} + \hat{\Sigma}_{Ji}) F_{iK} + E_K D_J\| N_K N_J. \tag{69}$$

Appendix B. The stress solution of film with a sinusoidal surface

Since constant electric field strength E_3 is applied along direction x_3 only (Fig. 1b), the Maxwell stresses $\hat{\sigma}_{ij}$ keep constant values in the film. The stress equilibriums are simplified,

$$\sigma_{ij,j} = -\hat{\sigma}_{ij,j} = 0 \quad (i,j = 1,3). \tag{70}$$

With $\varepsilon_{22} = 0$, one obtains the plane-strain constitutive relations from Eq. (11),

$$\sigma_{11} = 2G\varepsilon_{11} + \lambda(\varepsilon_{11} + \varepsilon_{33}) - \frac{a_2 E_3^2}{2}, \tag{71a}$$

$$\sigma_{33} = 2G\varepsilon_{33} + \lambda(\varepsilon_{11} + \varepsilon_{33}) - \frac{(a_1 + a_2) E_3^2}{2}, \tag{71b}$$

$$\sigma_{13} = 2G\varepsilon_{13}, \tag{71c}$$

$$\sigma_{22} = \lambda(\varepsilon_{11} + \varepsilon_{33}) - \frac{a_2 E_3^2}{2}. \tag{71d}$$

The metal-film mismatch stress is applied in the far-field, which requires

$$\sigma_{11} = \sigma_{11}^0 \quad \text{for } x_1 \to \pm\infty. \tag{72}$$

From Eqs. (4b) and (8c), the traction free boundary and interface conditions reduce to

$$\sigma_{11} n_1 + \sigma_{31} n_3 = 0 - \hat{\sigma}_{11} n_1 - \hat{\sigma}_{31} n_3 = \frac{\epsilon_0 E_3^2}{2} n_1, \tag{73a}$$

$$\sigma_{13} n_1 + \sigma_{33} n_3 = 0 - \hat{\sigma}_{13} n_1 - \hat{\sigma}_{33} n_3 = -\frac{\epsilon_0 E_3^2}{2} n_3. \tag{73b}$$

For the metal-film interface, $n_1 = 0$ and $n_3 = -1$, we derive

$$\sigma_{31} = 0, \quad \sigma_{33} = -\frac{\epsilon_0 E_3^2}{2} \quad \text{at } x_3 = -h_0. \tag{74a, b}$$

As $\omega a \ll 1$, $n_1 = -h_{,1}/\sqrt{1 + (h_{,1})^2} \approx a\omega \sin\omega x_1$ and $n_3 = 1/\sqrt{1 + (h_{,1})^2} \approx 1$ on the wavy film–environment interface (Eq. (19)). Hence, we found

$$\sigma_{11}(a\omega \sin\omega x_1) + \sigma_{31} = \frac{\epsilon_0 E_3^2}{2}(a\omega \sin\omega x_1), \tag{75a}$$

$$\sigma_{13}(a\omega \sin\omega x_1) + \sigma_{33} = -\frac{\epsilon_0 E_3^2}{2} \quad \text{at } x_3 = \Delta h(x_1; t). \tag{75b}$$

The plane-strain elastic above can be resolved by introducing a revised Ariy stress function, φ, which is related to the Cauchy stress tensor by

$$\sigma_{11} = \varphi_{,33} + \sigma_{11}^0, \quad \sigma_{33} = \varphi_{,11} - \frac{\epsilon_0 E_3^2}{2}, \quad \sigma_{13} = -\varphi_{,13}. \tag{76a, b, c}$$

The equilibrium conditions (Eq. (70)) thereupon are satisfied automatically, and the strain compatibility requires

$$\nabla^4\varphi=0. \tag{77}$$

For the given cosine wave surface, the general solution for Eq. (77) is found,

$$\varphi=(C_1\exp(-\omega x_3)+C_2x_3\exp(-\omega x_3)+C_3\exp(\omega x_3)+C_4x_3\exp(\omega x_3))\cos\omega x_1, \tag{78}$$

where C_1, C_2, C_3, and C_4 are coefficients. Substituting Eq. (78) into Eq. (76), one obtains the stress fields,

$$\begin{aligned}\sigma_{11}=&(C_1\omega^2\exp(-\omega x_3)+C_2\omega^2x_3\exp(-\omega x_3)-2C_2\omega\exp(-\omega x_3)\\&+C_3\omega^2\exp(\omega x_3)+C_4\omega^2x_3\exp(\omega x_3)+2C_4\omega\exp(\omega x_3))\cos\omega x_1+\sigma_{11}^0,\end{aligned} \tag{79a}$$

$$\sigma_{33}=-(C_1\exp(-\omega x_3)+C_2x_3\exp(-\omega x_3)+C_3\exp(\omega x_3)+C_4x_3\exp(\omega x_3))\omega^2\cos\omega x_1-\frac{\epsilon_0E_3^2}{2}, \tag{79b}$$

$$\sigma_{13}=(-C_1\omega\exp(-\omega x_3)-C_2\omega x_3\exp(-\omega x_3)+C_2\exp(-\omega x_3)+C_3\omega\exp(\omega x_3)+C_4\omega x_3\exp(\omega x_3)+C_4\exp(\omega x_3))\omega\sin\omega x_1. \tag{79c}$$

Substituting Eq. (79) into Eqs. (74) and (75), and with $\omega a\ll 1$, one achieves

$$(-C_1\omega\exp(\omega h_0)+C_2\omega h_0\exp(\omega h_0)+C_2\exp(\omega h_0)+C_3\omega\exp(-\omega h_0)-C_4\omega h_0\exp(-\omega h_0)+C_4\exp(-\omega h_0))\omega\sin\omega x_1=0, \tag{80a}$$

$$-(C_1\exp(\omega h_0)-C_2h_0\exp(\omega h_0)+C_3\exp(-\omega h_0)-C_4h_0\exp(-\omega h_0))\omega^2\cos\omega x_1=0, \tag{80b}$$

$$(-C_1\omega+C_2+C_3\omega+C_4)\omega\sin\omega x_1=\left(\frac{\epsilon_0E_3^2}{2}-\sigma_{11}^0\right)a\omega\sin\omega x_1, \tag{80c}$$

$$-(C_1+C_3)\omega^2\cos\omega x_1=0. \tag{80d}$$

The coefficients C_1–C_4 are determined by solving Eq. (80)), and are given by

$$C_1=-C_3=-\frac{2a\omega h_0^2\left(\sigma_{11}^0-\frac{\epsilon_0E_3^2}{2}\right)}{-2-4\omega^2h_0^2+\exp(2\omega h_0)+\exp(-2\omega h_0)}, \tag{81a}$$

$$C_2=\frac{a\left(\sigma_{11}^0-\frac{\epsilon_0E_3^2}{2}\right)(1-2\omega h_0-\exp(-2\omega h_0))}{-2-4\omega^2h_0^2+\exp(2\omega h_0)+\exp(-2\omega h_0)}, \tag{81b}$$

$$C_4=\frac{a\left(\sigma_{11}^0-\frac{\epsilon_0E_3^2}{2}\right)(1+2\omega h_0-\exp(2\omega h_0))}{-2-4\omega^2h_0^2+\exp(2\omega h_0)+\exp(-2\omega h_0)}. \tag{81c}$$

Substituting Eq. (81) into Eq. (79), one obtains the stress fields in the film. With Eq. (71), the strain fields can be further derived.

Appendix C. Combined material properties and morphology coefficient

Two combined material parameters are defined,

$$\alpha=\frac{\left(3\frac{a_1}{\epsilon_0}+3\frac{a_2}{\epsilon_0}-1\right)\left(\frac{a_1}{\epsilon_0}+\frac{a_2}{\epsilon_0}-1\right)}{2(2G+\lambda)} \tag{82}$$

and

$$\beta=\frac{\left[-\left(2G\frac{a_2}{\epsilon_0}-\lambda\frac{a_1}{\epsilon_0}\right)-2(\lambda+G)\right]\left(2G\frac{a_2}{\epsilon_0}-\lambda\frac{a_1}{\epsilon_0}\right)}{2G(2G+\lambda)(G+\lambda)}. \tag{83}$$

In order to determine these properties, we need the values for the permittivity ϵ_0 as well as the two electrostrictive parameters a_1 and a_2. The permittivity is a product of the relative dielectric constant ϵ and the permittivity of free space ϵ_V, $\epsilon_0=\epsilon\epsilon_V$. The two electrostrictive parameters are difficult to measure in experiments, however, they can also be expressed in terms of ϵ and ϵ_V based on a theoretical framework (Shkel and Klingenberg, 1998), $a_1=-\frac{2}{5}(\epsilon-1)^2\epsilon_V$ and $a_2=[-\frac{1}{3}(\epsilon-1)(\epsilon+2)+\frac{2}{15}(\epsilon-1)^2]\epsilon_V$. From Eq. (82), we derive

$$\alpha=\frac{(3\epsilon^2+4\epsilon-2)(9\epsilon^2+2\epsilon-6)}{50(2G+\lambda)\epsilon^2}=\frac{(1+\nu)(1-2\nu)(3\epsilon^2+4\epsilon-2)(9\epsilon^2+2\epsilon-6)}{50E(1-\nu)\epsilon^2}. \tag{84}$$

Since $\epsilon > 1$ and $2G+\lambda > 0$ for most oxide films, we found $\alpha > 0$. α is plotted in Fig. 3, which monotonically increases with enlarging ϵ or decreasing ν.

The combined material property β (Eq. (83)) can also be expressed as

$$\beta = \frac{2(1+\nu)[\epsilon(-1+4\nu)-(4-6\nu)](\epsilon-1)}{25E\epsilon^2(-1+\nu)}[\epsilon^2(-1+4\nu)+2\epsilon(1+\nu)+(4-6\nu)]. \tag{85}$$

For different Poisson ratio, the value of β is depicted in Fig. 4. β is positive when ϵ is small, which turns to negative values for larger ϵ. The critical dielectric constant ϵ_{cr} at the turning points first increases then decreases with increasing ν.

χ is the morphology coefficient as a function of the product ωh_0 (i.e., the normalized average thickness $\overline{h}_0$),

$$\chi = \frac{-4\omega h_0+\exp(2\omega h_0)-\exp(-2\omega h_0)}{-2-4\omega^2 h_0^2+\exp(2\omega h_0)+\exp(-2\omega h_0)} = \frac{-4\overline{h}_0+\exp(2\overline{h}_0)-\exp(-2\overline{h}_0)}{-2-4\overline{h}_0^2+\exp(2\overline{h}_0)+\exp(-2\overline{h}_0)}. \tag{86}$$

Fig. 5 depicts the value of χ, which is positive for any $\overline{h}_0$. When $\overline{h}_0 \gg 1$, $\chi \approx 1$. When $\overline{h}_0 \ll 1$, $\chi \approx 2/\overline{h}_0$ by using Taylor series.

References

Abeyaratne, R., Knowles, J.K., 1990. On the driving traction acting on a surface of strain discontinuity in a continuum. J. Mech. Phys. Solids 38 (3), 345–360.
Du, X., Srolovitz, D.J., 2004. Electrostatic field-induced surface instability. Appl. Phys. Lett. 85, 4917–4919.
Eringen, A.C., Maugin, G.A., 1990. Electrodynamics of Continua I-Foundations and Solid Media. Springer-Verlag Press.
Harper, J.E., 1999. Analysis of nonlinear electroelastic continua with electric conduction. Ph.D. Thesis, Massachusetts Institute of Technology.
Heuer, A.H., Kahn, H., Cross, L.E. Electrostrictive stresses and breakdown of thin passive films on stainless steel, Private Communication.
James, R.D., 2002. Configurational forces in magnetism with application to the dynamics of a small-scale ferromagnetic shape memory alloy. Continuum Mech. Thermodyn. 14, 55–86.
Jiang, Q., 1994. On the driving traction acting on a surface of discontinuity within a continuum in the presence of electromagnetic fields. J. Elast. 34, 1–21.
Jiang, Q., Cao, C.F., 2010. Axisymmetric stress in an electrostrictive hollow cylinder under electric loading. Acta Mech. 211, 309–321.
Kaesche, H., 1960. Anodic marginal current and pitting of aluminium in alkaline solution of neutral salts. J. Phys. Chem. 26, 138–142.
Kuang, Z., 2009. Internal energy variational principles and governing equations in electroelastic analysis. Int. J. Solids Struct. 46, 902–911.
Leckie, H.P., Uhlig, H.H., 1966. Environmental factors affecting the critical potential for pitting in 18-8 stainless steel. J. Electrochem. Soc. 113 (12), 1262–1267.
Liang, J., Suo, Z., 2001. Stress-assisted reaction at a solid–fluid interface. Interface Sci. 9, 95–104.
Martin, F.J., Lemieux, E.J., Newbauer, T.M., Bayles, R.A., Natishan, P.M., Kahn, H., Michal, G.M., Ernst, F., Heuer, A.H., 2007. Carburization-induced passivity of 316 l austenitic stainless steel. Electrochem. and Solid St. 10 (12), C76–C78.
Martin, F.J., Natishan, P., Lemieux, E.J., Newbauer, T.M., Rayne, R.J., Bayles, R.A., Kahn, H., Michal, G.M., Ernst, F., Heuer, A.H., 2009. Enhanced corrosion resistance of stainless steel carburized at low temperature. Metall. Mater. Trans. A 40A, 1805–1810.
Maugin, G.A., Trimarco, C., 1997. Driving force on phase transition fronts in thermoelectroelastic crystals. Math. and Mech. Solids 2, 199–214.
McCafferty, E., 2010. Introduction to Corrosion Science. Springer.
McMeeking, R.M., Landis, C.M., Jimeneza, S.M.A., 2007. A principle of virtual work for combined electrostatic and mechanical loading of materials. Int. J. Non Linear Mech. 42, 831–838.
Prevost, J.H., Baker, T.J., Liang, J., Suo, Z., 2001. A finite element method for stress-assisted surface reaction and delayed fracture. Int. J. Solids Struct. 38, 5185–5203.
Sato, N., 1971. A theory for breakdown of anodic oxide films on metals. Electrochim. Acta 16, 1683–1692.
Shkel, Y.M., Klingenberg, D.J., 1998. Electrostriction of polarizable materials: comparison of models with experimental data. J. Appl. Phys. 83, 7834–7843.
Song, W., Yang, F., 2006. Surface evolution of a stressed elastic layer in an electric field. J. Phys. D Appl. Phys. 39, 4634–4642.
Srolovitz, D.J., 1989. On the stability of surfaces of stressed solids. Acta Metall. 37, 621–625.
Suo, Z., 1997. Motions of microscopic surfaces in materials. Adv. Appl. Math. 33, 193–294.
Wernick, S., Pinner, R., Sheasby, P.G., 1987. The Surface Treatment and Finishing of Aluminum and its Alloys. ASM International.
Yang, F., 2006. Stress-induced surface instability of an elastic layer. Mech. Mater. 38, 111–118.
Yu, H.H., Suo, Z., 2000. Stress-dependent surface reactions and implications for a stress measurement technique. J. Appl. Phys. 87 (3), 1211–1218.